NANO LETTERS

pubs.acs.org/NanoLett Letter

Influence of Orbital Character on the Ground State Electronic Properties in the van Der Waals Transition Metal Iodides VI_3 and CrI_3

Alessandro De Vita ¶ Thao Thi Phuong Nguyen ¶ Roberto Sant Gian Marco Pierantozzi Danila Amoroso Chiara Bigi Vincent Polewczyk Giovanni Vinai Loi T. Nguyen Tai Kong Jun Fujii Ivana Vobornik Nicholas B. Brookes Giorgio Rossi Robert J. Cava Federico Mazzola Kunihiko Yamauchi Silvia Picozzi and Giancarlo Panaccione

Cite This: https://doi.org/10.1021/acs.nanolett.2c01922 Read Online

ACCESS | Metrics & More | Article Recommendations | Supporting Information

ABSTRACT: Two-dimensional van der Waals magnetic semiconductors display emergent chemical and physical properties and hold promise for novel optical, electronic and magnetic "few-layers" functionalities. Transition-metal iodides such as CrI_3 and VI_3 are relevant for future electronic and spintronic applications; however, detailed experimental information on their ground state electronic properties is lacking often due to their challenging chemical environment. By combining X-ray electron spectroscopies and first-principles calculations, we report a complete determination of CrI_3 and VI_3 electronic ground states. We show that the transition metal-induced orbital filling drives the stabilization of distinct electronic phases: a wide bandgap in CrI_3 and a Mott insulating state in VI_3. Comparison of surface-sensitive (angular-resolved photoemission spectroscopy) and bulk-sensitive (X-ray absorption spectroscopy) measurements in VI_3 reveals a surface-only V^{2+} oxidation state, suggesting that ground state electronic properties are strongly influenced by dimensionality effects. Our results have direct implications in band engineering and layer-dependent properties of two-dimensional systems.

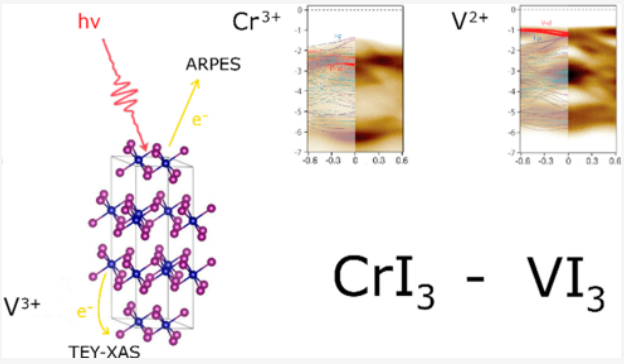

KEYWORDS: *Electronic structure, van der Waals systems, ARPES, DFT*

Research on two-dimensional (2D) van der Waals (vdW) materials has been recently boosted by the discovery of layer-dependent long-range magnetic order,[1−4] Dirac physics[5,6] as well as Mott transitions.[7] Among 3d transition-metal vdW semiconductors, CrI_3 and VI_3 have attracted significant attention, as they undergo structural and electronic transitions as a function of temperature, net long-range magnetization within layers, and in the case of CrI_3 layered antiferromagnetism.[8−14] The importance of dimensionality effects has been recognized and for this reason the majority of experimental and theoretical work has focused on monolayers and few-layers films. However, both the interplay of dimensionality with relevant interactions, such as spin−orbit coupling (SOC), and the possible crossover of 3D vs 2D electronic properties are not well understood. In this respect, open questions include: (i) the role of Coulomb interaction and SOC in determining the 3d electronic states and their long- and short-range ordered collective excitations,[15] (ii) if and how the orbital filling in the electronic ground state is modified at the surface, (iii) what are the changes in the bandwidth and of the hybridization of halogen and transition metal states when dimensionality is reduced. These issues need to be addressed, since they have a significant impact in the potential electronic and spintronic applications, and their control may drive the realization of tailored heterostructures.[16,17]

The crystal structure of MI_3 (M = Cr, V) is characterized by one M cation surrounded by six I anions, arranged in edge-sharing octahedra. Within the planes, the M atoms are arranged in a honeycomb geometry (Figure 1a). CrI_3 undergoes a structural transition at $T_{S,CrI3}$ = 220 K from the high-temperature monoclinic structure to the low-temperature rhombohedral structure $R\bar{3}$, while VI_3 changes from the rhombohedral structure $R\bar{3}$ above $T_{S,VI3}$ = 79 K to a monoclinic phase below the transition temperature.[18] Concerning the electronic structure, for VI_3 two different descriptions were proposed in literature: (i) a metallic ground

Received: May 11, 2022
Revised: August 23, 2022

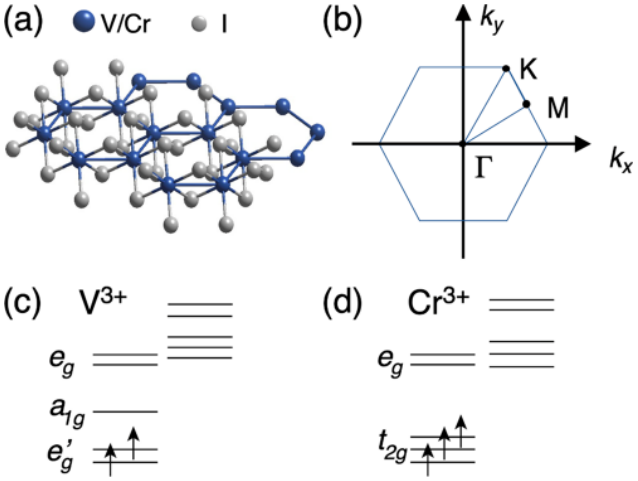

Figure 1 (a) Crystal structure of CrI_3 and VI_3 monolayers. (b) Two-dimensional Brillouin zone. Crystal-field splitting and related electron filling for (c) Cr and (d) V.

state, in which the a_{1g} orbital state is fully occupied, and the doubly degenerate e_g' orbital state is half occupied;[9,19,20] (ii) a Mott-insulating ground state, in which the e_g' state is fully occupied, while the a_{1g} state is unoccupied.[17,21] This last picture appears to be consistent with a previous experimental measure of the optical band gap in VI_3[22] and a recent spectroscopic investigation;[23] indeed, no density of states at the Fermi level has been detected. The authors suggest that despite the trigonal distortion in this system being small and thus alone not being able to significantly split the t_{2g} orbital state into e_g' and a_{1g} states, the energy gap is opened by the additional on-site Coulomb interaction contribution. However, a firm characterization of the ground state of VI_3 has not been reached yet.

As for CrI_3, it has been proposed that a surface structural relaxation may explain the onset of bulk ferromagnetism vs few-layers antiferromagnetism;[24] it has also been argued that parallel spin states are energetically favored in both stacking configurations, and the result strongly depends on the on-site Coulomb energy employed in the calculations.[17] Hence, a better understanding of the surface electronic configuration and orbital occupation/arrangement would be helpful to better understand how interlayer interaction affects electronic states.

Motivated by the above issues, in this Letter we report on the determination of the electronic ground state of 3D-crystalline CrI_3 and VI_3, by combining different depth-sensitive electron spectroscopies with density functional theory (DFT) calculations for single layers. We observe that in CrI_3 a wide band gap is opened between majority spin e_g and t_{2g} states, whereas in VI_3 the t_{2g} orbital state is split into (filled) e_g' and (empty) a_{1g} orbital states with a narrower band gap between them, consistently with DFT predictions. Surface-sensitive angular-resolved photoemission spectroscopy (ARPES) data reveal the stabilization of a different ground state in VI_3 at the surface, characterized by a V^{2+} valence and an occupied a_{1g} band, where the bandgap lies between the octahedral-split a_{1g} and the higher-lying empty e_g states. In contrast, the 3^+ oxidation state measured both for bulk CrI_3 and VI_3 by X-ray absorption spectroscopy (XAS). Resonant photoemission spectroscopy (ResPES) data, compared to atom- and orbital-resolved density of states obtained from DFT, provide consistent evidence of the orbital character of the different valence band contributions, revealing that the orbital character itself has a profound influence on the ground state electronic properties. The good consistency between experimental data and DFT single-layer calculations suggest that interlayer interactions are less important in determining the stable electronic configuration for both CrI_3 and VI_3.

vdW crystals are quasi-two-dimensional systems with little interaction along the *c*-axis layer stacking direction. The extreme surface-sensitivity of ARPES when performed with photon energies in the 20−55 eV range (from 5 to 10 Å,[25] corresponding to a single layer unit) allows to study the single-layer electronic structure of MI_3, referring to the surface-projected BZ reported in Figure 1b. We also report, for reference, in Figure 1c,d the expected crystal field splitting and related electronic filling for Cr^{3+} and V^{3+}, respectively.

XAS measurements across the V and Cr $L_{2,3}$ edges (Figure 2a,b) confirm the 3^+ oxidation state of bulk CrI_3 and VI_3. As a matter of fact, the line shape and photon energy of L_3 and L_2 edges of the former are fully consistent with previous measurements on CrI_3,[26,27] while V $L_{2,3}$ edges of the latter closely resemble those of other vanadium compounds with a V^{3+} valence state such as V_2O_3, including the characteristic V 2p to V 3d empty t_{2g} transitions in the near-edge regions at 514 and 522 eV.[27,28] The spectra of both compounds are unaffected by contamination as they were cleaved *in-vacuo*.

XAS spectra are intrinsically integrated over a thickness of 4−6 nm of material,[29] and as such it does not retain information coming from the very first layer of CrI_3 and VI_3. The direct surface analysis and investigation of the energy and the overall symmetry of the electronic states of VI_3 and CrI_3 was addressed by collecting k_x−k_y photoemission intensity maps at constant energy (see Figure 2c−f) and energy-momentum spectra, (see Figure 2k−l). Experimental results were compared to DFT calculated electronic structures, where the U value was changed in the range between 0 and 3 eV (see SI, Methods and Figure S1) for both materials, seeking the best agreement with ARPES data. The calculations were performed for a single-layer with FM configuration, i.e. the magnetic ground state in monolayer form for VI_3 and CrI_3, both with and without SOC. The magnetization direction, when SOC was included, was out-of-plane, consistently with the orientation of the magnetic moments. We note that our ARPES data were measured above the Curie temperature; nevertheless, a much better agreement is found with spin-polarized DFT, rather than with nonmagnetic DFT calculations. The latter would in fact result in a metallic ground state, inconsistent with experimental results on these materials. Local magnetic correlations may actually occur even above the Curie temperature and this is implied by the good agreement of experimental data and spin-polarized DFT, even in the absence of long-range magnetic ordering.

Our experimental data show the existence of a sizable bandgap (the distance between the valence band maximum and the conduction band minimum) for both systems and allow us to evaluate the bandgap energies to be larger than 0.9 eV for VI_3 and 1.35 eV for CrI_3. These values have been obtained by comparing ARPES data to the experimentally determined Fermi level (see Methods). It is important to underline that the experimental bandgap values are lower limits for the full bandgap, as ARPES detects occupied electron-density of states (DOS) only; in addition, the presence of small charging effects of cleaved surfaces[30−32] cannot be excluded. The latter are common and well-understood in ARPES

https://doi.org/10.1021/acs.nanolett.2c01922
Nano Lett XXXX XXX XXX−XXX

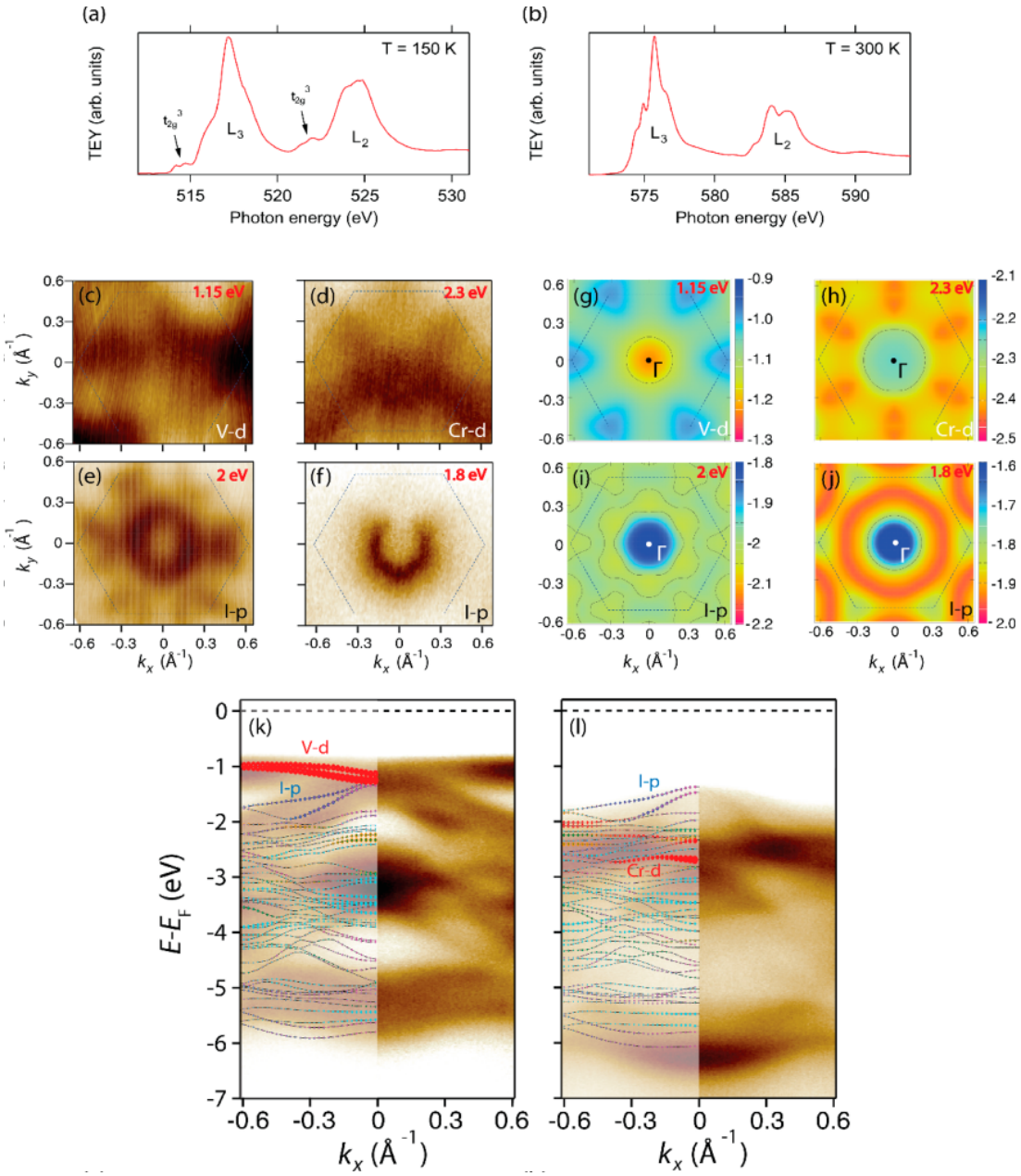

Figure 2 XAS spectrum of CrI_3 (a) over the Cr $L_{2,3}$ edge (T = 300 K), and VI_3 (b) over the V $L_{2,3}$ edge (T = 150 K). ARPES isoenergetic k_x−k_y maps of VI_3 (T = 150 K, $h\nu$ = 32 eV) at (c) 1.15 eV and (e) 2 eV, and CrI_3 (T = 300 K, $h\nu$ = 41 eV) at (d) 2.3 eV and (f) 1.8 eV, highlight the 3-fold symmetry of V/Cr-d states and the 6-fold symmetry of I-p states. The energy in red in the top-right corner of each map pinpoints the binding energy of the isoenergetic cut. DFT calculation of the total energy map with contours shown as black lines for specific energies of VI_3, (g) 1.15 eV, (i) 2 eV and CrI_3, (h) 2.3 eV, (j) 1.8 eV. Dashed lines in each image represent the 2D hexagonal first Brillouin zone. The energy in red in the top right corner of each map is the binding energy of the isoenergetic cut. ARPES spectra of (k) VI_3 (T = 150 K, $h\nu$ = 32 eV) and (l) CrI_3 (T = 300 K, $h\nu$ = 32 eV) along the Γ−K direction. Theoretical band structures with FM configuration and SOC for VI_3 (GGA+U, U = 2 eV) and CrI_3 (bare GGA) monolayers are superimposed on experimental data. The colors highlighting the bands represent the following components for V/Cr d-orbital, red denotes d_{3z2-r2}, green denotes d_{xz} and d_{yz}, yellow denotes d_{xy} and $d_{x_2-y_2}$. For I p-orbital, gray denotes p_z, magenta denotes p_y, blue denotes p_z.

measurements of insulating compounds and can determine an artifactual rigid shift of the Fermi level of a few hundreds of millielectronvolts, without further changes in the band structure, as we verified in our measurements (see SI Figure S2). We note that we cannot use DFT calculations (as reported in SI Figure S3) for quantitative comparison, as the underestimate of band gaps is a well-known DFT problem in treating excited states.[33] Nevertheless, a good agreement with previous experimental results is found, yielding a similar value obtained from optical measurements for CrI_3[34] and also both from optical[12,22] and spectroscopic[23] measurements for VI_3.

From Figure 2, we note that the overall electronic structures of VI_3 and CrI_3 show several similarities. In fact, the 3*d* electronic states originating from V or Cr give rise to similar nearly dispersionless features in the VB, whose intensity is prominent in the collected spectra (Figure 2k,l). On the other

https://doi.org/10.1021/acs.nanolett.2c01922
Nano Lett XXXX XXX XXX−XXX

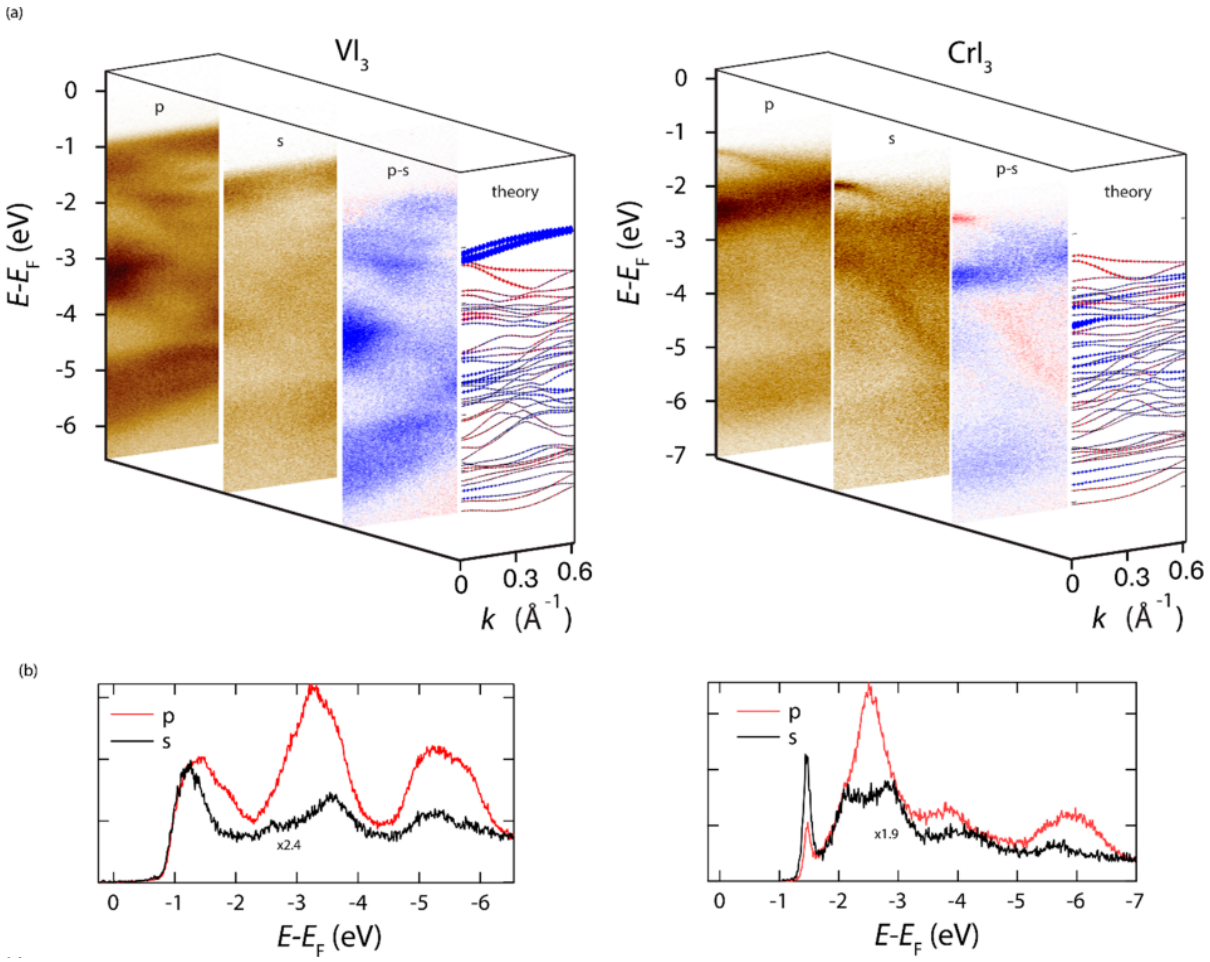

Figure 3 (a) VI_3 (left) and CrI_3 (right) spectra as a function of light polarization (p-polarization, s-polarization, difference p−s). p-polarized light has an out-of-plane component, while s-polarized light is completely in-plane. The "theory" panel displays the DFT band structure; a blue color indicates bands with out-of-plane component, while a red color emphasizes in-plane bands. (b) Angle-integrated spectra of VI_3 (left) and CrI_3 (right) evidencing polarization-dependent intensity of specific band features.

hand, the I-derived 5p orbitals are very dispersive and the orbital-mixing is strong for both VI_3 and CrI_3. The orbital character of these bands, as inferred from DFT, shows that the SOC is crucial for explaining the observed energy-momentum spectra. The effect of SOC modulates the band structure involving the V/Cr d_{z2-3r2} and I p_x-p_y orbitals at binding energies of ∼1 eV in VI_3 and around 2.5 eV in CrI_3. Moreover, the inclusion of SOC is relevant in closing the gap between V a_{1g} and I p bands at Γ (see SI Figure S1).

Despite I p bands being fairly similar, our results show that VI_3 and CrI_3 behave in a different way from the electronic point of view. To emphasize this point, we carried out polarization-dependent measurements on both compounds. p-polarized light has both in-plane and out-of-plane components of the wavevector with respect to the sample surface, whereas s-polarized light has only the in-plane component. By exploiting the light polarization dependence we are thus selectively sensitive to in- and out-of- plane orbitals (Figure 3). For VI_3, we clearly see in Figure 3a that the orbitals contributing to the spectroscopic signal at ∼1 eV are mostly out of plane, that is, those with a_{1g} character. A value of U = 2 eV is thus found to best simulate our data. Higher values of U would shift the V a_{1g} states up toward the Fermi level, opening a gap between them and the I bands which is not observed in the experiment (Figure S1h). Lower values of U, instead, would place V d_{xz} and d_{yz} orbitals at an energy of ∼1 eV (Figure S1e-f) which is inconsistent with the data.

ARPES results for CrI_3 are in striking difference with those shown above for VI_3. First, from Figure 3a we deduce that bands at 2.5 eV BE are ascribed to the out-of-plane d_{3z2-r2} orbitals. Second, we observe that, as soon as U values different from zero are introduced in the DFT calculations, those orbitals move to higher BEs (Figure S1n−p), a feature that is not observed by ARPES. This can be interpreted as follows. CrI_3 exhibits $t_{2g}-e_g$ crystal-field splitting of d states; the different orbital filling of Cr^{3+} ions compared to V^{3+} results in a t_{2g} level completely filled by majority electrons. The orbital splitting between e_g and t_{2g} orbital states is sufficiently large in this case to stabilize a fully insulating state, even in the absence of a finite U-value within the DFT+U approach.

Another relevant difference between the two compounds is that DFT calculations compare well with ARPES spectra with the exception of the a_{1g} orbital filling of VI_3. The a_{1g} are clearly revealed as filled states by ARPES, while are predicted to be empty by DFT consistently with a V^{3+} ionic charge. On top of this, XAS results also indicate a V^{3+} valency of the bulk. This peculiar behavior is nevertheless clearly revealed by ARPES, which probes just the topmost layer of the material, therefore

https://doi.org/10.1021/acs.nanolett.2c01922
Nano Lett XXXX XXX XXX−XXX

including intrinsic and extrinsic surface effects like relaxation and defect-doping effects that can be responsible of the local electron filling of the a_{1g} band. We thus suggest that a different ground state, characterized by a V^{2+} orbital filling, stabilizes at the surface: it turns out that the gap between filled and empty states observed in ARPES measurements is opened by the octahedral crystal field, rather than that by the bulk trigonal crystal field splitting of a_{1g} and e_g' levels. On the other hand, CrI_3 does not show any evidence of a different surface electronic environment.

In Figure 2c–f, we note that the constant energy ARPES maps for VI_3 and CrI_3 display a different symmetry in connection with the orbital character of the electronic states. I 5p states display an apparent 6-fold symmetry, while V and Cr 3d states show a 3-fold symmetric pattern, differently from DFT results (reported in Figure 2g–j). The 3-fold symmetry of V 3d states is highlighted also in SI Figure S4. Indeed, the expected trigonal symmetry is not necessarily reproduced in our single-layer calculations, since the primitive cell encompasses two layers. In previous works, it has been suggested that such a pattern could be connected with the onset of the ferromagnetic ground state,[23] that breaks time-reversal symmetry when VI_3 undergoes the magnetic transition. At the surface, this combines with the loss of inversion symmetry, giving rise to a $P-T$ symmetry-breaking system. Our ARPES data (150 K for VI_3, 300 K for CrI_3) were collected at sample temperatures well above the Curie point (CrI_3, $T_{C,CrI3}$ = 61 K; VI_3, $T_{C,VI3}$ = 50 K), and suggest a different interpretation with respect to the one given in ref 23. The reduction of symmetry of ARPES constant energy maps with respect to DFT results may be ascribed to surface effects, that are not accounted for in the DFT simulations of VI_3 and CrI_3 single-layers (i.e., not for semi-infinite crystals). However, we cannot rule out the existence of magnetic fluctuations and their role in breaking time-reversal symmetry.

The relevance of short-range magnetic interactions in vdW magnetic materials, including VI_3, has been pointed out by numerous studies.[13,35−38] Well above the Curie temperature, thermal fluctuations randomly orient the electron spins in the valence band, but the nonmagnetic ground state can be locally described in terms of orbital filling of the TM states by majority electrons. The occurrence of magnetic fluctuations well above the Curie point in the absence of long-range order is well-documented for correlated materials;[39−42] the observed narrow bandwidth of V- and Cr-derived 3d bands hints at the importance of electron−electron interactions as well. Furthermore, V- and Cr-projected states would be more affected by short-range correlation effects, while the I contribution to the magnetic moment is negligible,[9] leaving the symmetry of I 5p states as dictated by the structure. The intralayer atomic arrangement does not change even at the structural transition that both crystals undergo at $T_{S,CrI3}$ = 220 K and $T_{S,VI3}$ = 78 K, involving only layer stacking. The comparison of calculations and surface-sensitive experimental data allows us to conclude that the band structure is largely unaffected across the structural transitions.

We also measured ResPES, exploiting the selective abrupt changes of photoionization cross sections, to identify the orbital contributions to the spectra. V 3d orbitals contributing to the bands at 1 eV BE, and similarly Cr 3d orbitals contributing to the bands at 2.5 eV BE, are resonantly enhanced when the photon energy reaches the photoionization threshold of the V and Cr 3p core levels, respectively. In this way, we experimentally probe the atomic character of the wave functions contributing to ARPES intensities. The large signal enhancement of the nondispersing bands when the photon energy coincides with the 3p edges (Figure 4a,c) is a direct signature of their V/Cr orbital nature, and can be mapped onto the DFT orbital projection of the DOS (Figure 4b,d).

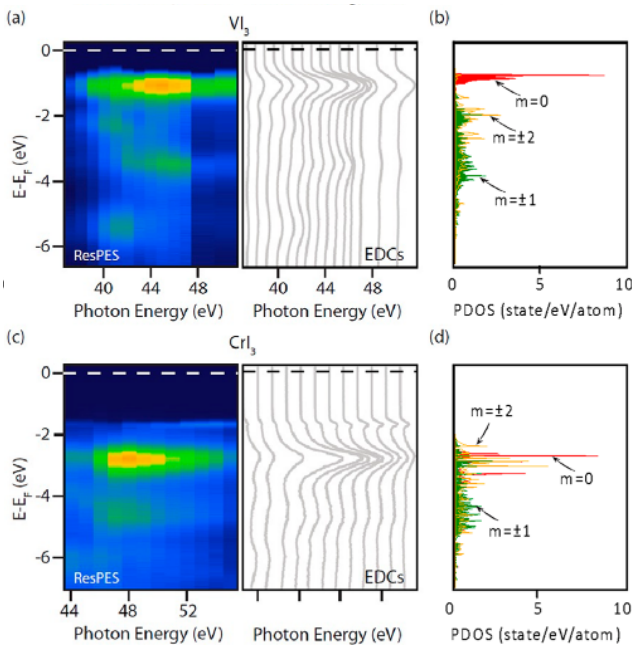

Figure 4 (a) ResPES in the first BZ for VI_3: the color map (left panels) displays the momentum-integrated photoemission intensity; the resonant EDCs (right panels) emphasize the band dispersion (or lack of) along the measured photon energy. (b) d-orbital projection DOS of VI_3; the color scale represents d orbital characters as follows: filled red, m = 0; filled green, m = 1; orange, m = 2. (c,d) Same as (a,b), but for CrI_3.

Photon energy dependent ARPES, such as ResPES, intrinsically also probes the k_z dispersion. The absence of dispersion of both V and Cr projected bands, highlighted by the EDC spectra (Figure 4a–c, right panel), indicates that those states are "2D-like" with negligible interlayer interaction (assuming no artifacts are introduced by rescaling the spectra to compensate charging effects). The consistency of ARPES results with single-layer calculations appears therefore strengthened.

In summary, we characterized the ground-state electronic structure of CrI_3 and VI_3: based on the excellent agreement between photoemission data (angle-resolved, light polarization-dependent and resonant) and DFT-calculated band dispersion and orbital-resolved density of states, we give evidence of how substantially different can be the orbital configuration of magnetic trihalides for different TM ions. CrI_3 shows a 3-fold t_{2g} orbital degeneracy and a wide bandgap, while VI_3 shows a Mott-insulator-like ground state with a_{1g}-e_g' orbital splitting and a narrower bandgap. Single-layer band structure calculations compare well with ARPES spectra suggesting weak electronic interaction between layers, including between the surface layer and the bulk. Moreover, the occupancy of the a_{1g} state at the surface of VI_3 indicates that its surface is stabilized by an unconventional V^{2+} state, at variance with the V^{3+} bulk valency. Therefore, future research in ultrathin films or

https://doi.org/10.1021/acs.nanolett.2c01922
Nano Lett XXXX XXX XXX−XXX

nanoparticles of MI_3 van der Waals materials with variable surface to bulk ratios should carefully explore the effective ionic configurations that determine their electronic properties and related potential functionalities.

■ ASSOCIATED CONTENT

Supporting Information

The Supporting Information is available free of charge at https://pubs.acs.org/doi/10.1021/acs.nanolett.2c01922.

Methods and experimental details, beamline specifications, additional calculations (PDF)

■ AUTHOR INFORMATION

Corresponding Author

Giancarlo Panaccione − *Laboratorio TASC, in Area Science Park, Istituto Officina dei Materiali (IOM)-CNR, I-34149 Trieste, Italy;* orcid.org/0000-0003-0122-4041; Email: panaccione@iom.cnr.it

Authors

Alessandro De Vita − *Laboratorio TASC, in Area Science Park, Istituto Officina dei Materiali (IOM)-CNR, I-34149 Trieste, Italy; Dipartimento di Fisica, Universita di Milano, I-20133 Milano, Italy;* orcid.org/0000-0001-9413-2810

Thao Thi Phuong Nguyen − *Institute of Scientific and Industrial Research, Osaka University, Osaka 567-0047, Japan; Department of Precision Engineering, Graduate School of Engineering, Osaka University, Osaka 565-0871, Japan*

Roberto Sant − *ESRF, The European Synchrotron, F-38043 Grenoble, France*

Gian Marco Pierantozzi − *Laboratorio TASC, in Area Science Park, Istituto Officina dei Materiali (IOM)-CNR, I-34149 Trieste, Italy;* orcid.org/0000-0002-5044-5716

Danila Amoroso − *Consiglio Nazionale delle Ricerche (CNR-SPIN), Unita di Ricerca presso Terzi c/o Universita "G. D Annunzio", 66100 Chieti, Italy; NanoMat/Q-mat/CESAM, Universit de Liege, B−4000 Liege, Belgium*

Chiara Bigi − *Laboratorio TASC, in Area Science Park, Istituto Officina dei Materiali (IOM)-CNR, I-34149 Trieste, Italy; School of Physics and Astronomy, University of St. Andrews, St. Andrews KY16 9SS, United Kingdom;* orcid.org/0000-0003-0977-3993

Vincent Polewczyk − *Laboratorio TASC, in Area Science Park, Istituto Officina dei Materiali (IOM)-CNR, I-34149 Trieste, Italy*

Giovanni Vinai − *Laboratorio TASC, in Area Science Park, Istituto Officina dei Materiali (IOM)-CNR, I-34149 Trieste, Italy;* orcid.org/0000-0003-4882-663X

Loi T Nguyen − *Department of Chemistry, Princeton University, Princeton, New Jersey 08540, United States;* orcid.org/0000-0003-1293-8613

Tai Kong − *Department of Chemistry, Princeton University, Princeton, New Jersey 08540, United States*

Jun Fujii − *Laboratorio TASC, in Area Science Park, Istituto Officina dei Materiali (IOM)-CNR, I-34149 Trieste, Italy*

Ivana Vobornik − *Laboratorio TASC, in Area Science Park, Istituto Officina dei Materiali (IOM)-CNR, I-34149 Trieste, Italy*

Nicholas B Brookes − *ESRF, The European Synchrotron, F-38043 Grenoble, France*

Giorgio Rossi − *Laboratorio TASC, in Area Science Park, Istituto Officina dei Materiali (IOM)-CNR, I-34149 Trieste, Italy; Dipartimento di Fisica, Universita di Milano, I-20133 Milano, Italy;* orcid.org/0000-0002-9330-7436

Robert J Cava − *Department of Chemistry, Princeton University, Princeton, New Jersey 08540, United States*

Federico Mazzola − *Laboratorio TASC, in Area Science Park, Istituto Officina dei Materiali (IOM)-CNR, I-34149 Trieste, Italy;* orcid.org/0000-0002-5380-4374

Kunihiko Yamauchi − *Institute of Scientific and Industrial Research, Osaka University, Osaka 567-0047, Japan; Department of Precision Engineering, Graduate School of Engineering, Osaka University, Osaka 565-0871, Japan;* orcid.org/0000-0002-9265-1091

Silvia Picozzi − *Consiglio Nazionale delle Ricerche (CNR-SPIN), Unita di Ricerca presso Terzi c/o Universita "G. D Annunzio", 66100 Chieti, Italy*

Complete contact information is available at: https://pubs.acs.org/10.1021/acs.nanolett.2c01922

Author Contributions

A.D.V., S.P., and G.P. designed the research; A.D.V., T.T.P.N., R.S., G.M.P., D.A., C.B., V.P., G.V., J.F., I.V., N.B.B., F.M., K.Y., S.P., and G.P. performed the research; some of the crystals were grown at Princeton University by R.J.C. and T.K.; A.D.V., T.T.P.N., R.S., G.M.P., D.A., C.B., V.P., G.V., N.B.B., G.R., F.M., K.Y., S.P., and G.P. analyzed data; T.T.P.N. and K.Y. performed calculations, discussing results with D.A. and S.P.; A.D.V., T.T.P.N., F.M., K.Y., S.P., and G.P. wrote the paper with contributions of all authors. All authors have given approval to the final version of the manuscript.

Author Contributions

¶A.D.V. and T.T.P.N. contributed equally.

Notes

The authors declare no competing financial interest.

■ ACKNOWLEDGMENTS

This work was performed in the framework of the Nanoscience Foundry and Fine Analysis (NFFA-MUR Italy) facility and was supported by JST-CREST (No. JPMJCR18T1). A part of the computation in this work, using the VASP code[43] in the GGA approximation[44], was performed by using the facilities of the Supercomputer Center, the Institute for Solid State Physics, the University of Tokyo and MASAMUNE-IMR, Center for Computational Materials Science, Institute for Materials Research, Tohoku University (Project No. 20K0045).

■ REFERENCES

(1) Gibertini, M.; Koperski, M.; Morpurgo, A. F.; Novoselov, K. S. Magnetic 2D materials and heterostructures. *Nature Nanotechnology* **2019**, *14*, 408.

(2) Samarth, N. Magnetism in flatland. *Nature* **2017**, *546*, 216.

(3) Butler, S. Z.; Hollen, S. M.; Cao, L.; Cui, Y.; Gupta, J. A.; Gutierrez, H. R.; Heinz, T. F.; Hong, S. S.; Huang, J.; Ismach, A. F.; Johnston-Halperin, E.; Kuno, M.; Plashnitsa, V. V.; Robinson, R. D.; Ruoff, R. S.; Salahuddin, S.; Shan, J.; Shi, L.; Spencer, M. G.; Terrones, M.; Windl, W.; Goldberger, J. E. Progresses, Challenges and Opportunities in Two-Dimensional Materials Beyond Graphene. *ACS Nano* **2013**, *7*, 2898.

(4) Mounet, N.; Gibertini, M.; Schwaller, P.; Campi, D.; Merkys, A.; Marrazzo, A.; Sohier, T.; Castelli, I. E.; Cepellotti, A.; Pizzi, G.; Marzari, N. Two-dimensional materials from high-throughput

computational exfoliation of experimentally known compounds. *Nat. Nanotechnol.* **2018**, *13*, 246−252.
(5) Yang, T. Y.; Wan, Q.; Yan, D. Y.; Zhu, Z.; Wang, Z. W.; Peng, C.; Huang, Y. B.; Yu, R.; Hu, J.; Mao, Z. Q.; Li, S.; Yang, S. A.; Zheng, H.; Jia, J. F.; Shi, Y. G.; Xu, N. Directional massless Dirac fermions in a layered van der Waals material with one-dimensional long-range order. *Nat. Mater.* **2020**, *19*, 27.
(6) Chen, L.; Stone, M. B.; Kolesnikov, A. I.; Winn, B.; Shon, W.; Dai, P.; Chung, J. H. Massless Dirac magnons in the two dimensional van der Waals honeycomb magnet CrCl3. *2D Materials* **2022**, *9*, 015006.
(7) Wang, Y. P.; Long, M. Q. Electronic and magnetic properties of van der Waals ferromagnetic semiconductor VI_3. *Phys. Rev. B* **2020**, *101*, 024411.
(8) Ke, L.; Katsnelson, M. I. Electron correlation effects on exchange interactions and spin excitations in 2D van der Waals materials. *npj Computational Materials* **2021**, *7*, 4.
(9) He, J.; Ma, S.; Lyu, P.; Nachtigall, P. Unusual Dirac half-metallicity with intrinsic ferromagnetism in vanadium trihalide monolayers. *Journal of Materials Chemistry C* **2016**, *4*, 2518.
(10) Huang, B.; Clark, G.; Navarro-Moratalla, E.; Klein, D. R.; Cheng, R.; Seyler, K. L.; Zhong, Di.; Schmidgall, E.; McGuire, M. A.; Cobden, D. H.; Yao, W.; Xiao, D.; Jarillo-Herrero, P.; Xu, X. Layer-dependent ferromagnetism in a van der Waals crystal down to the monolayer limit. *Nature* **2017**, *546*, 270−273.
(11) Gati, E.; Inagaki, Y.; Kong, T.; Cava, R. J.; Furukawa, Y.; Canfield, P. C.; Bud Ko, S. L. Multiple ferromagnetic transitions and structural distortion in the van der Waals ferromagnet VI_3 at ambient and finite pressures. *Phys. Rev. B* **2019**, *100*, 094408.
(12) Son, S.; Coak, M. J.; Lee, N.; Kim, J.; Kim, T. Y.; Hamidov, H.; Cho, H.; Liu, C.; Jarvis, D. M.; Brown, P. A. C.; Kim, J. H.; Park, C. H.; Khomskii, D. I.; Saxena, S. S.; Park, J. G. Bulk properties of the van der Waals hard ferromagnet VI_3. *Phys. Rev. B* **2019**, *99*, 041402.
(13) Tian, S.; Zhang, J. F.; Li, C.; Ying, T.; Li, S.; Zhang, X.; Liu, K.; Lei, H. Ferromagnetic van der Waals Crystal VI_3. *J. Am. Chem. Soc.* **2019**, *141*, 5326.
(14) McGuire, M. A.; Dixit, H.; Cooper, V. R.; Sales, B. C. Coupling of Crystal Structure and Magnetism in the Layered, Ferromagnetic Insulator CrI_3. *Chem. Mater.* **2015**, *27*, 612.
(15) Reyes-Retana, J. A.; Cervantes-Sodi, F. Spin-orbital effects in metal-dichalcogenide semiconducting monolayers. *Sci. Rep.* **2016**, *6*, 24093.
(16) Zollner, K.; Gmitra, M.; Fabian, J. Swapping Exchange and Spin-Orbit Coupling in 2D van der Waals Heterostructures. *Phys. Rev. Lett.* **2020**, *125*, 196402.
(17) Nguyen, T. T. P.; Yamauchi, K.; Oguchi, T.; Amoroso, D.; Picozzi, S. Electric-field tuning of the magnetic properties of bilayer VI_3: A first-principles study. *Phys. Rev. B* **2021**, *104*, 014414.
(18) Huang, C.; Wu, F.; Yu, S.; Jena, P.; Kan, E. Discovery of twin orbital-order phases in ferromagnetic semiconducting VI_3 monolayer. *Phys. Chem. Chem. Phys.* **2020**, *22*, 512.
(19) Yang, K.; Fan, F.; Wang, H.; Khomskii, D. I.; Wu, H. VI_3: A two-dimensional Ising ferromagnet. *Phys. Rev. B* **2020**, *101*, 100402.
(20) Kong, T.; Stolze, K.; Timmons, E. I.; Tao, J.; Ni, D.; Guo, S.; Yang, Z.; Prozorov, R.; Cava, R. J. VI_3 − a New Layered Ferromagnetic Semiconductor. *Adv. Mater.* **2019**, *31*, 1808074.
(21) Zhou, Z.; Kumar Pandey, S.; Feng, J. Dynamical correlation enhanced orbital magnetization in VI_3. *Phys. Rev. B* **2021**, *103*, 035137.
(22) Wang, Z.; Gutiérrez-Lezama, I.; Ubrig, N.; Kroner, M.; Gibertini, M.; Taniguchi, T.; Watanabe, K.; Imamoglu, A.; Giannini, E.; Morpurgo, A. Very large tunneling magnetoresistance in layered magnetic semiconductor CrI_3. *Nat. Commun.* **2018**, *9*, 2516.
(23) Kundu, A. K.; Liu, Y.; Petrovic, C.; Valla, T. Valence band electronic structure of the van der Waals ferromagnetic insulators: VI_3 and CrI_3. *Sci. Rep.* **2020**, *10*, 15602.
(24) Frisk, A.; Duffy, L. B.; Zhang, S.; van der Laan, G.; Hesjedal, T. Magnetic X-ray spectroscopy of two-dimensional CrI_3 layers. *Mater. Lett.* **2018**, *232*, 5−7.
(25) Seah, M. P.; Dench, W. A. Quantitative electron spectroscopy of surfaces: A standard data base for electron inelastic mean free paths in solids. *Surf. Interface Anal.* **1979**, *1* (1), 2−11.
(26) Kim, D.-H.; Kim, K.; Ko, K.-T.; Seo, J.; Kim, J. S.; Jang, T.-H.; Kim, Y.; Kim, J.-Y.; Cheong, S.-W.; Park, J.-H. Giant Magnetic Anisotropy Induced by Ligand L-S Coupling in Layered Cr Compounds. *Phys. Rev. Lett.* **2019**, *122*, 207201.
(27) de Groot, F. M. F.; Fuggle, J. C.; Thole, B. T.; Sawatzky, G. A. 2p x-ray absorption of 3d transition-metal compounds: An atomic multiplet description including the crystal field. *Phys. Rev. B* **1990**, *42*, 5459.
(28) Caputo, M.; Jandke, J.; Cappelli, E.; Chaluvadi, S. K.; Bonini Guedes, E.; Naamneh, M.; Vinai, G.; Fujii, J.; Torelli, P.; Vobornik, I.; Goldoni, A.; Orgiani, P.; Baumberger, F.; Radovic, M.; Panaccione, G. Metal to insulator transition at the surface of V2O3 thin films: An in-situ view. *Appl. Surf. Sci.* **2022**, *574*, 151608.
(29) Frazer, B. H.; Gilbert, B.; Sonderegger, B. R.; De Stasio, G. The probing depth of total electron yield in the sub-keV range: TEY-XAS and X-PEEM. *Surf. Sci.* **2003**, *537*, 161−167.
(30) Harris, L.; Fiasson, J. Direct determination of surface potential on sodium chloride single crystals: I. Analysis of measurements. *Journal of Physics C: Solid State Physics* **1985**, *18* (25), 4845−62.
(31) Wintle, H. J. Interpretation of atomic force microscope (AFM) signals from surface charge on insulators. *Measurement Science and Technology* **1997**, *8*, 508.
(32) Engelhardt, J.; Dabringhaus, H.; Wandelt, K. Atomic force microscopy study of the $CaF_2(111)$ surface: from cleavage via island to evaporation topographies. *Surf. Sci.* **2000**, *448* (2−3), 187−200.
(33) Giuliani, G.; Vignale, G. *Quantum Theory of the Electron Liquid*; Cambridge University Press: Cambridge, 2005.
(34) Dillon, J. F., Jr.; Olson, C. E. Magnetization, Resonance, and Optical Properties of the Ferromagnet CrI_3. *J. Appl. Phys.* **1965**, *36*, 1259.
(35) McGuire, M. A.; Clark, G.; Santosh, K. C.; Chance, W. M.; Jellison, G. E., Jr.; Cooper, V. R.; Xu, X.; Sales, B. C. Magnetic behavior and spin-lattice coupling in cleavable van der Waals layered $CrCl_3$ crystals. *Physical Review Materials* **2017**, *1*, 014001.
(36) Suzuki, M.; Gao, B.; Koshiishi, K.; Nakata, S.; Hagiwara, K.; Lin, C.; Wan, Y. X.; Kumigashira, H.; Ono, K.; Kang, S.; Kang, S.; Yu, J.; Kobayashi, M.; Cheong, S.-W.; Fujimori, A. Coulomb-interaction effect on the two-dimensional electronic structure of the van der Waals ferromagnet $Cr_2Ge_2Te_6$. *Phys. Rev. B* **2019**, *99*, No. 161401.
(37) Zeisner, J.; Alfonsov, A.; Selter, S.; Aswartham, S.; Ghimire, M. P.; Richter, M.; van den Brink, J.; Buchner, B.; Kataev, V. Magnetic anisotropy and spin-polarized two-dimensional electron gas in the van der Waals ferromagnet $Cr_2Ge_2Te_6$. *Phys. Rev. B* **2019**, *99*, 165109.
(38) Zeisner, J.; Mehlawat, K.; Alfonsov, A.; Roslova, M.; Doert, T.; Isaeva, A.; Buchner, B.; Kataev, V. Electron spin resonance and ferromagnetic resonance spectroscopy in the high-field phase of the van der Waals magnet $CrCl_3$. *Physical Review Materials* **2020**, *4*, 064406.
(39) Pramanik, A. K.; Banerjee, A. Griffiths phase and its evolution with Mn-site disorder in the half-doped Manganite $Pr_{0.5}Sr_{0.5}Mn_{1-y}Ga_yO_3$ (y = 0.0, 0.025 and 0.05). *Phys. Rev. B* **2010**, *81*, 024431.
(40) Jiang, W.; Zhou, X. Z.; Williams, G.; Mukovskii, Y.; Glazyrin, K. Griffiths phase and critical behavior in single-crystal $La_{0.7}Ba_{0.3}MnO_3$: Phase diagram in $La_{1-x}Ba_xMnO_3$ ($x \leq 0.33$). *Phys. Rev. B* **2008**, *77*, 064424.
(41) Pezhumkattil Palakkal, J.; Lekshmi, P. N.; Thomas, S.; Suresh, K. G.; Varma, M. R. Observation of high-temperature magnetic transition and existence of ferromagnetic short-range correlations above transition in double perovskite La_2FeMnO_6. *RSC Adv.* **2015**, *5*, 105531.
(42) Panaccione, G.; Vobornik, I.; Fujii, J.; Krizmancic, D.; Annese, E.; Giovanelli, L.; Maccherozzi, F.; Salvador, F.; de Luisa, A.; Benedetti, D.; Gruden, A.; Bertoch, P.; Polack, F.; Cocco, D.; Sostero, G.; Diviacco, B.; Hochstrasser, M.; Maier, U.; Pescia, D.; Back, C. H.; Greber, T.; Osterwalder, J.; Galaktionov, M.; Sancrotti, M.; Rossi, G.

https://doi.org/10.1021/acs.nanolett.2c01922
Nano Lett XXXX XXX XXX−XXX

Advanced photoelectric effect experiment beamline at Elettra: A surface science laboratory coupled with Synchrotron Radiation. *Rev. Sci. Instrum.* **2009**, *80*, 043105.
(43) Kresse, G.; Furthmuller, J. Efficient iterative schemes for ab initio total-energy calculations using a plane-wave basis set. *Phys. Rev. B* **1996**, *54*, 11169.
(44) Perdew, J. P.; Burke, K.; Ernzerhof, M. Generalized Gradient Approximation Made Simple. *Phys. Rev. Lett.* **1996**, *77*, 3865.

https://doi.org/10.1021/acs.nanolett.2c01922
Nano Lett XXXX XXX XXX−XXX